Arabian Journal for Science and Engineering
https://doi.org/10.1007/s13369-026-11364-1

TECHNICAL NOTE–CIVIL ENGINEERING

Full-Scale Field Investigation of Lateral Load–Deformation Behavior of Concrete-Encased Steel Piles for Solar Panel Foundations

Iman Golpazir[1,2] · Ali Dehghanbanadaki[1,2] · Reza Akherati[3] · Anahita Akherati[3,4] · Alireza Rezaee[5]

Received: 26 November 2025 / Accepted: 23 April 2026

Abstract

Despite the rapid expansion of large-scale solar farms, field-based evidence quantifying how soil shear strength interacts with composite pile geometry under lateral loading remains limited. This study addresses this gap through 60 full-scale lateral load tests conducted on concrete-encased steel piles at the Meymand Solar Farm in Iran. Piles reinforced with UNP 100 and UNP 140 steel sections and embedded to depths of 1.2 m and 1.7 m was tested under lateral loading along the strong (L1) and weak (L2) axes. Results demonstrate pronounced anisotropy, with L1 capacities consistently exceeding L2, yielding an average L1/L2 ratio of 2.31. Quadratic regression reveals a strong correlation between L1 and friction angle (R2 = 0.93), indicating that strong-axis resistance is governed primarily by mobilized soil shear strength. In contrast, L2 shows a weak correlation with friction angle, confirming that weak-axis behavior is dominated by pile bending stiffness rather than soil strength. Increasing the steel core size from UNP 100 to UNP 140 produced larger capacity gains than increasing embedment depth, particularly for L1. Comparison with Broms' theoretical ultimate capacity shows that weak-axis service loads at 10 mm displacement mobilize only 16–87% of the ultimate soil resistance, providing a substantial safety margin. These findings advance current knowledge by providing rare full-scale field evidence that decouples the governing mechanisms of strong- and weak-axis lateral resistance in composite solar piles and offers quantitative, design-oriented guidance for optimizing pile section and embedment in dense granular soils.

Keywords Concrete-encased steel piles · Lateral load test · Dense granular soil · Anisotropic behavior

1 Introduction

The shift toward renewable energy has accelerated in recent years, driven by growing concerns over environmental impacts, the gradual depletion of fossil fuel reserves, and the need for sustainable long-term energy solutions [1–4]. Among these alternatives, solar photovoltaic (PV) systems have emerged as one of the fastest-growing renewable technologies due to their scalability, low environmental footprint, and capacity for decentralized power generation [5–7]. In many regions, including Iran, rising electricity demand alongside governmental incentives for renewable energy development has significantly boosted the large-scale deployment of solar farms [8–11].

The long-term performance and stability of solar photovoltaic installations are critically dependent on the design and construction quality of their foundation systems [12, 13]. These foundations provide the necessary structural support for the mounting assemblies, ensuring that panels remain within permissible displacement limits under both operational and extreme loading conditions, particularly those induced by wind-generated lateral forces. In large-scale solar farms, inadequate foundation performance can result in excessive tilting, panel misalignment, or structural failure, ultimately reducing energy yield and increasing maintenance costs [14]. Various foundation solutions have been implemented worldwide—including driven steel piles, precast concrete footings, and cast-in-place concrete piles—each

✉ Ali Dehghanbanadaki
Dehghanbanadaki.a@iau.ac.ir

1 Department of Civil Engineering, Dmv.C, Islamic Azad University, Damavand, Iran

2 Research Center of Concrete and Soil, Dmv.C, Islamic Azad University, Damavand, Iran

3 ZaminRun Ravesh Geotechnical Company, Tehran, Iran

4 Departments of Civil Engineering, University of Tehran, Tehran, Iran

5 Jarfpey Geotechnical Company, Tehran, Iran

Published online: 11 May 2026

offering specific advantages depending on local geotechnical and environmental conditions [15].

In operational environments, foundation systems are subjected to a combination of vertical loads from the self-weight of the mounting assemblies, uplift forces generated by wind suction, and dynamic loads induced by temperature fluctuations and operational vibrations. Among these, lateral loads—primarily resulting from wind pressures acting on panel surfaces—are particularly critical, as they can cause lateral displacement, rotation, or progressive loosening of the foundation–soil interface [16–20]. Inadequate resistance to such lateral forces can lead to structural instability, panel misalignment, reduced energy efficiency, and increased maintenance requirements over the service life of the installation.

The determination of the load–deformation behavior of pile foundations has been a pivotal aspect of geotechnical engineering practice [21–26], particularly for structures subjected to significant wind or seismic forces [27–29]. In engineering design, this performance is typically evaluated using a combination of analytical models and experimental approaches, each aimed at predicting foundation response under varying soil conditions and loading scenarios [30, 31].

Analytical evaluations of pile performance under lateral loads often rely on the p–y method, which defines the nonlinear relationship between soil resistance (p) and lateral deflection (y) at specific depths [32–38]. This approach incorporates factors such as soil type, relative density, depth variation, and loading rate, making it applicable to diverse geotechnical conditions. In dense sands and gravels, the high relative density and interparticle interlock produce rapid mobilization of passive resistance at small displacements, resulting in a steep initial slope on the p–y curve and indicating high initial stiffness. As lateral deflection increases, particle rearrangement and dilation gradually reduce confinement, leading to progressive stiffness degradation and a transition to a softer response until the ultimate resistance is reached. Consequently, the curve exhibits pronounced initial rigidity followed by gradual softening under larger loads. Although widely adopted in practice, the predictive accuracy of the p–y method depends heavily on empirical parameters derived from generic soil profiles, which may lead to significant error when applied to specific sites without calibration. This limitation underscores the importance of conducting full-scale lateral load tests to obtain reliable site-specific soil–pile interaction data and to refine p–y formulations for local geotechnical conditions.

Although numerous experimental, analytical, and numerical investigations have examined the lateral behavior of pile foundations, the majority of existing studies have primarily focused on homogeneous pile sections, idealized soil profiles, or small-scale model testing. In many cases, lateral resistance has been evaluated without explicitly distinguishing between strong- and weak-axis loading directions or quantifying the resulting anisotropic response, particularly for composite concrete piles reinforced with steel cores that are increasingly used in solar photovoltaic foundations. Moreover, while soil shear strength parameters are widely recognized as influential in lateral pile performance, their direct correlation with directional lateral capacity, based on site-specific friction angle measurements, has rarely been established using full-scale field data. As a result, current design practices often rely on generalized assumptions that do not clearly distinguish between soil-controlled and section-controlled lateral resistance mechanisms. Therefore, there is a clear need for field-based studies that systematically investigate directional lateral behavior in composite piles and explicitly relate lateral capacity to measured soil friction angles, in order to provide more reliable, design-oriented guidance for solar foundation systems in dense granular soils.

The objective of this study is to investigate the lateral load–displacement behavior of single concrete pile foundations used in large-scale solar photovoltaic installations in dense granular soils, with particular emphasis on the relationship between lateral capacity and the soil friction angle. Field testing was conducted at the Meymand Solar Farm in Kerman Province, Iran, on sixty single concrete piles with varying lengths and cross-sections. The study aims to quantify pile performance under lateral loading in both strong-axis (L1) and weak-axis (L2) directions, evaluate the influence of geometric parameters such as pile length and section size, and establish empirical correlations between lateral loads (L1 and L2) and an equivalent friction angle for the surrounding dense sand and gravel. Additionally, the study seeks to verify the safety margins of the serviceability design criteria by comparing the experimental weak-axis results against theoretical ultimate capacities derived from Broms' method. These site-specific load–displacement relationships and design correlations are intended to support the development and calibration of reliable foundation design approaches for solar farm structures subjected to significant wind-induced lateral forces.

2 Methodology

2.1 Methodology Clarification

The methodological framework adopted in this study was designed to ensure direct reproducibility, clear physical interpretation, and relevance to serviceability-controlled solar foundation design. The approach is based on full-scale field testing, thereby avoiding scale effects and constitutive assumptions inherent in small-scale or numerical studies. All piles were tested under static monotonic lateral loading applied at a consistent elevation above ground, with boundary conditions representing free-head pile behavior typical of solar mounting systems. Two orthogonal loading directions were considered, corresponding to the strong (L1) and weak (L2) axes of the composite concrete–steel section, in order to explicitly capture directional stiffness effects. Material and soil parameters were obtained from site-specific geotechnical investigations and laboratory testing, including Standard Penetration Tests and direct shear tests, rather than assumed or calibrated values from the literature. The soil friction angle (ϕ) used in the analysis represents the average value over the pile embedment depth at each test location, reflecting local variability in dense granular deposits. While no parametric sensitivity analysis was performed, the experimental program inherently captures sensitivity through systematic variation of embedment depth, section stiffness, loading direction, and friction angle across 60 tests. Overall, this methodology is particularly suitable for the present study as it isolates soil-controlled and structure-controlled mechanisms using measurable field parameters, providing transparent, design-oriented insight into the lateral behavior of composite piles in dense granular soils.

2.2 Case Study Information

All experimental investigations were conducted within the Meymand Solar Farm, situated in Kerman Province, Iran. This region has recently witnessed an accelerated demand for renewable energy solutions, underscoring the strategic significance of large-scale solar panel installations. The project encompassed comprehensive components, including photovoltaic panel structural design, preliminary geotechnical investigations, and full-scale lateral testing, all tailored to address the specific geotechnical and environmental conditions prevalent at the Meymand site (https://zamin-run.com/en). To develop a reliable characterization of the subsurface conditions, a systematic drilling program was undertaken. A total of 30 boreholes were drilled across the solar farm site, facilitating a detailed evaluation of soil stratigraphy and essential geotechnical properties. The distribution of borehole depths and locations are presented in Fig. 1 (a) and (b).

2.3 Test Configuration and Experimental Program

The experimental program was designed to systematically isolate the effects of pile embedment depth and core section geometry on lateral bearing capacity. The study utilized composite piles consisting of concrete shafts reinforced with centrally placed cold-formed U-shaped steel sections (UNP series). Two specific core profiles were selected : UNP 100 and UNP 140. The UNP 100 section (nominal depth 100 mm, web thickness ~ 5 mm, flange width ~ 50 mm) represents a relatively slender reinforcement with lower bending stiffness. In contrast, the UNP 140 section (nominal depth 140 mm, with increased web and flange dimensions) provides significantly higher flexural rigidity and a larger second moment of area, particularly about the strong axis.

The selection of the UNP 100 and UNP 140 steel sections was based on practical design considerations and prevailing construction practices for solar photovoltaic foundations in Iran. These two profiles are among the most commonly available cold-formed U-shaped sections used by local contractors for concrete-encased solar piles and represent a realistic range of structural stiffness employed in practice.

To facilitate direct comparison, the 60 tests were organized into 30 comparative pairs. Within each pair, the embedment depth was held constant while the core section varied (one pile reinforced with UNP 100 and the corresponding partner with UNP 140). This configuration allowed for the quantification of the “section effect” under identical soil and depth conditions. To simultaneously evaluate the “depth effect,” the target embedment depths alternated between pairs: odd-numbered pairs (1, 3, …, 29) were tested at a shallow depth of 120 cm, while even-numbered pairs (2, 4, …, 30) were tested at a deeper embedment of 170 cm. The tests were labeled sequentially from TS-1 to TS-60, where each pair consists of an odd-numbered test TS-X and the subsequent even-numbered test TS-Y (e.g., Pair 1 comprises TS-1 and TS-2). A schematic view of the piles and statistical summary of the testing matrix are provided in Fig. 2 (a) and (b).

2.4 Loading and Measurement Setup

The testing program included vertical tension tests, lateral tension tests in the direction parallel to the web axis of the section, and lateral tension tests in the direction perpendicular to the web axis of the section. The vertical tension tests were not considered in this research, as they were outside the defined scope of the study. To minimize the influence of reaction forces generated during load application, the distance between the crane holding the load cell and each pile was maintained at greater than approximately 3 m. Applied loads were measured using a digital load cell with a capacity of 10,000 kgf and an accuracy of 5 kgf. Displacement changes were recorded using precision gauges with an accuracy of 0.01 mm, mounted on special magnetic bases at locations specified in the testing guidelines. Figure 3 (a) to (e) depicts the made piles and loading conditions.

Fig. 1 (**a**) Borehole depths (**b**) Borehole Locations

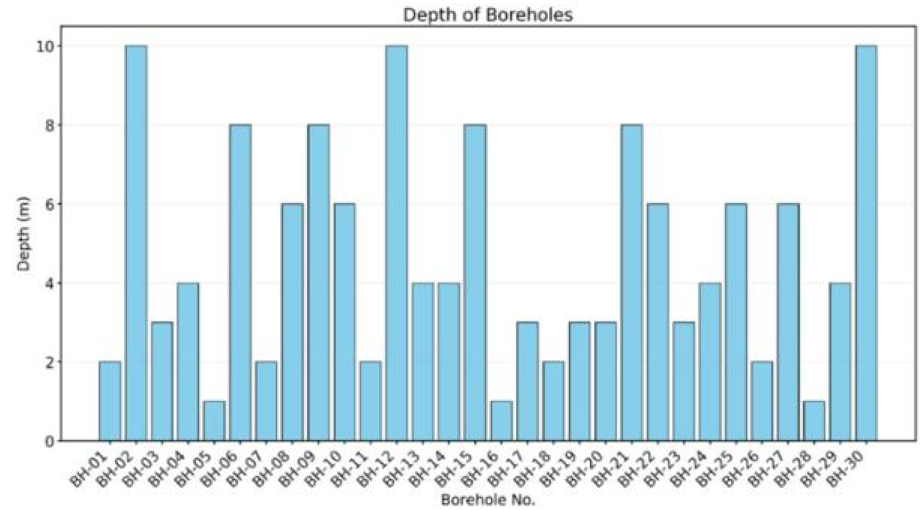

(a)

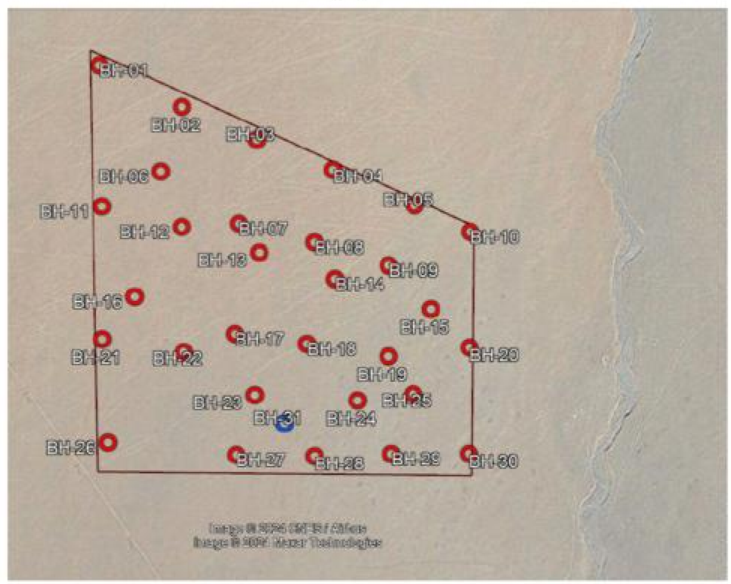

(b)

3 Results and Discussions

3.1 Geotechnical Properties of the Site

Figure 4(a) and 4(b) presents the borehole locations, the spatial distribution of organic soil thickness, and a representative geotechnical log from a trial pit. The subsurface stratigraphy typically consists of a thin surficial sandy–clayey layer underlain by approximately 60 cm of cohesive clay. Below this overburden, the profile transitions into deep, dense granular deposits comprising alternating strata of well-graded gravel (GW), poorly graded gravel (GP), and well-graded gravel with silt (GW-GM), interbedded with intermediate layers of poorly graded sand (SP), as classified by the Unified Soil Classification System (USCS).

Standard penetration test (SPT) results yielded average blow counts (N-values) ranging between 50 and 60 across the site, confirming the presence of dense, coarse-grained soils with high relative density. The interpreted average friction angle (ϕ) along the pile embedment depth varied from approximately 32–43°. While the site is consistently dense, this range represents a measurable variation in shear strength. Consequently, rather than treating the soil conditions as uniform, this study explicitly incorporates this variability into the analysis. By developing regression-based relationships between the measured lateral capacities (L1 and L2) and the specific friction angle at each test location, the analysis captures the interplay between structural geometry and local soil strength. This approach provides a more rigorous basis for interpreting the load–displacement behavior and refines the

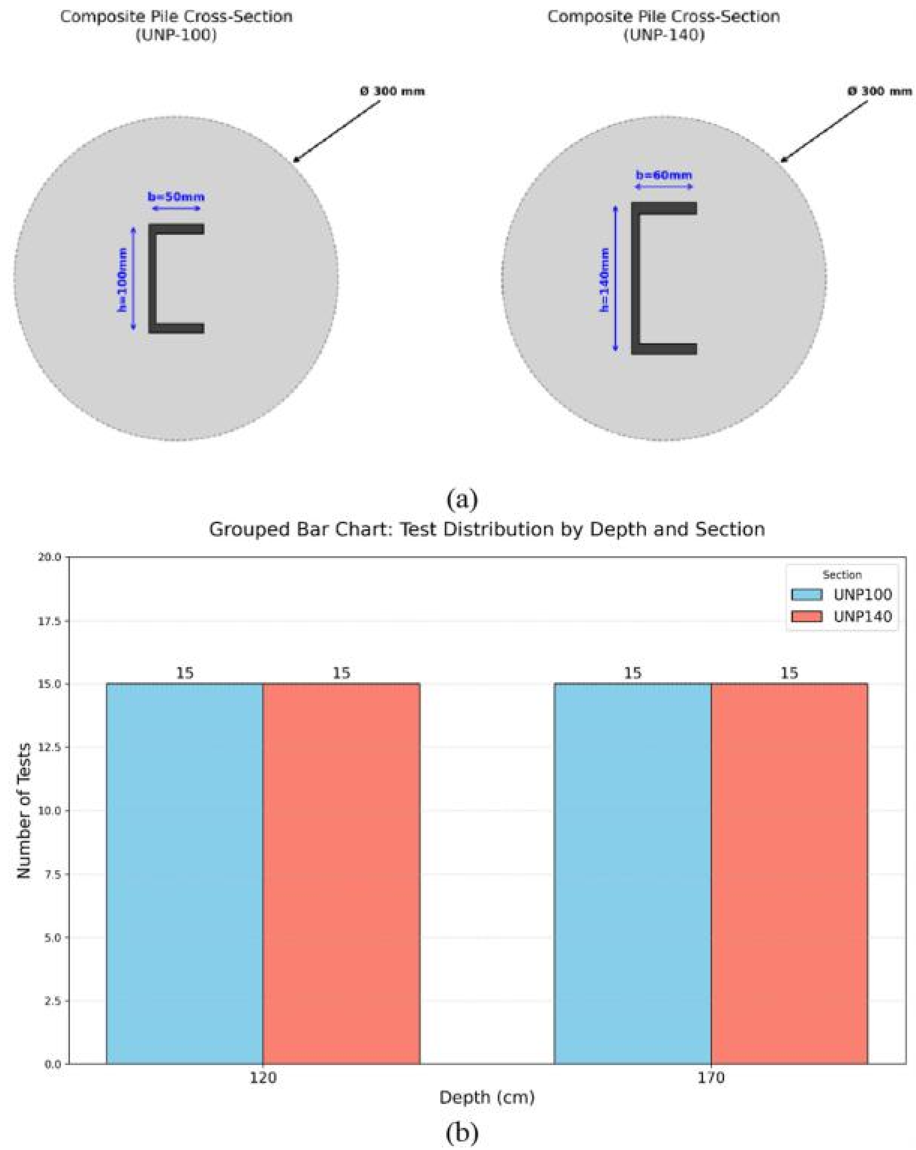

Fig. 2 (**a**) Section of the piles (**b**) Statistical information of the tests

design recommendations for solar pile foundations in heterogeneous granular soils.

3.2 Load displacement behavior of the piles

Figure 5 depicts load displacement behavior of the piles (TS-2). It should be mentioned that no piles experienced structural and geotechnical failure during testing, and as observed from the trend in Fig. 5, the load–displacement responses maintained a stable progression without abrupt drops in capacity. For each test, the values of L1 and L2 were selected at the load corresponding to a lateral displacement of 10 mm, ensuring a consistent basis for comparison. In the case of TS-2 (Section: UNP140, Length: 120 cm), the curve shows that L1 values remained higher than L2 throughout loading, with the final recorded capacities being 1.79 ton for L1 and 1.18 ton for L2, indicating greater stiffness and resistance in the primary load direction. The initial portion of the curve demonstrates a relatively steep slope, typical of dense soil support conditions, followed by gradual softening as displacement increases. All other piles tested exhibited similar overall trends in their load-–displacement responses, confirming the general behavioral pattern observed in TS-2.

Final lateral load of the piles (UNP 100 – L1) in Fig. 6 shows the spatial distribution of the final lateral resistance values (in tons) for piles with UNP 100 sections loaded in the L1 direction, mapped across different test zones at the site. The contour map illustrates localized variations in pile capacity, with warmer colors indicating zones of higher load demand and cooler shades representing lower resistance. As illustrated, the highest recorded values approach 1.05 ton in

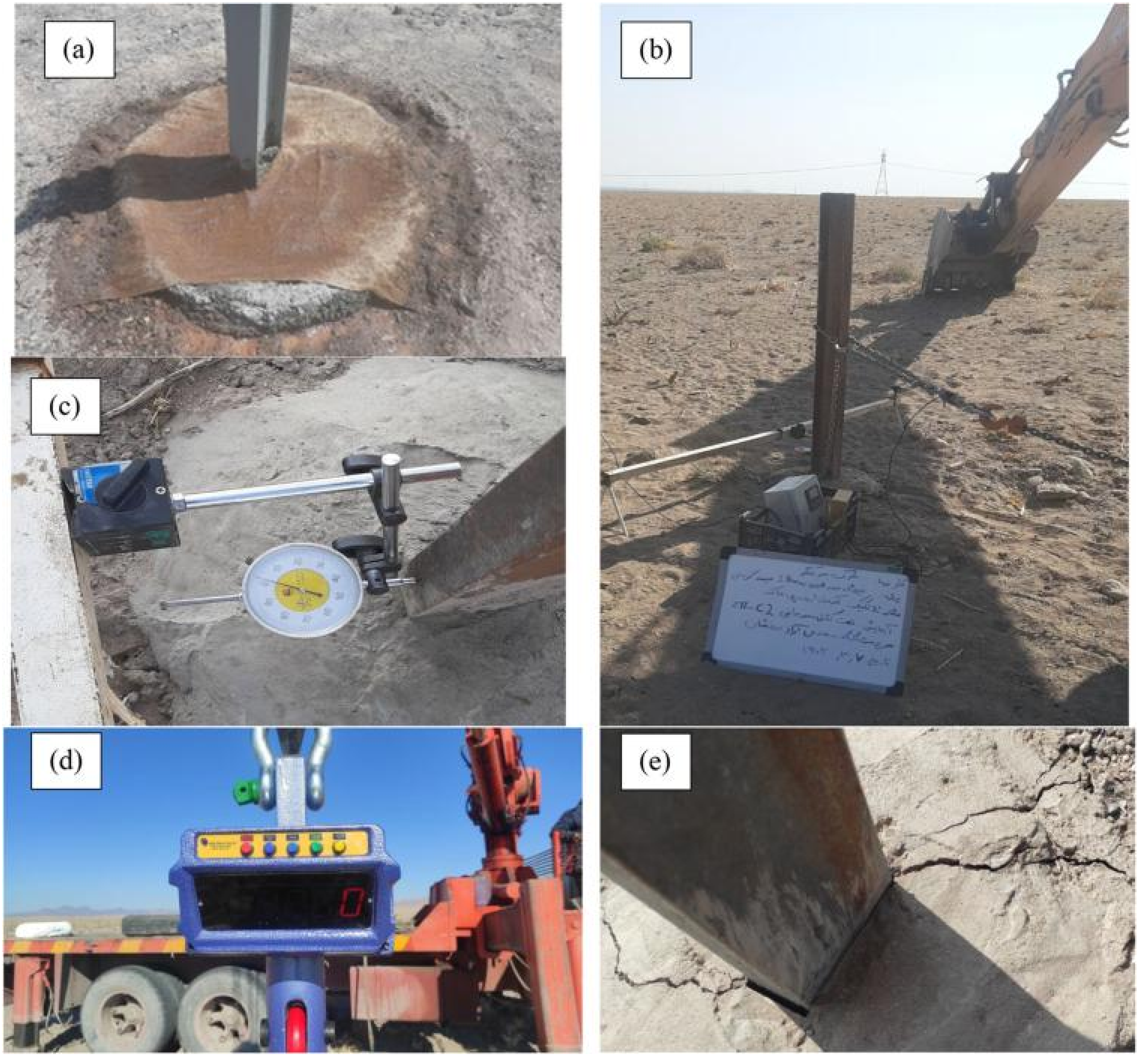

Fig.3 (**a**) Preparation of concrete pile (**b**) Lateral loading (**c**) LVDT (**d**) Loading system (**e**) Failure moment of piles

Zone 13, while some areas such as Zone 4 exhibit lower values around 0.55 ton.

3.3 Comparative Analysis of Lateral Load Performance of Piles

Figure 7(a) and 7(b) illustrates the final lateral loads obtained for L1 and L2 across all tests, as well as the corresponding L1/L2 ratios. As shown in Fig. 7 a, L1values consistently exceed L2 for all piles, confirming higher lateral capacity in the strong-axis loading direction. The maximum recorded L1 was 2.81 T and the minimum was 1.02 T, while L2 ranged from 0.45 T to 1.18 T, resulting in mean capacities of 1.73 T for L1 and 0.78 T for L2. In Fig. 7b, the L1/L2 ratio varies between 1.23 and 4.02, with an average of 2.31, indicating that strong-axis resistance is typically more than twice that of the weak-axis direction. Local peaks in the ratio plot represent cases where section geometry and soil–pile interaction effects significantly favored strong-axis performance, while lower ratios suggest more balanced behavior between directions. Overall, these trends across all piles reinforce the anisotropic lateral resistance resulting from both pile cross-sectional properties and installation conditions, consistent with the response patterns observed in individual load–displacement curves such as Fig. 6.

Figure 8 shows the correlation between L1 and L2 capacities for all tested piles. Each point represents final loads at 10 mm displacement, with UNP 100 piles in blue and UNP 140 piles in red. While both load directions exhibit a moderate positive correlation ($R = 0.49$), it was expected that a higher correlation coefficient would be detected due to the shared influence of soil properties on both directions. However, several parameters contributed to the lower-than-expected value, including anisotropy in pile section stiffness, localized variations in soil density and particle arrangement,

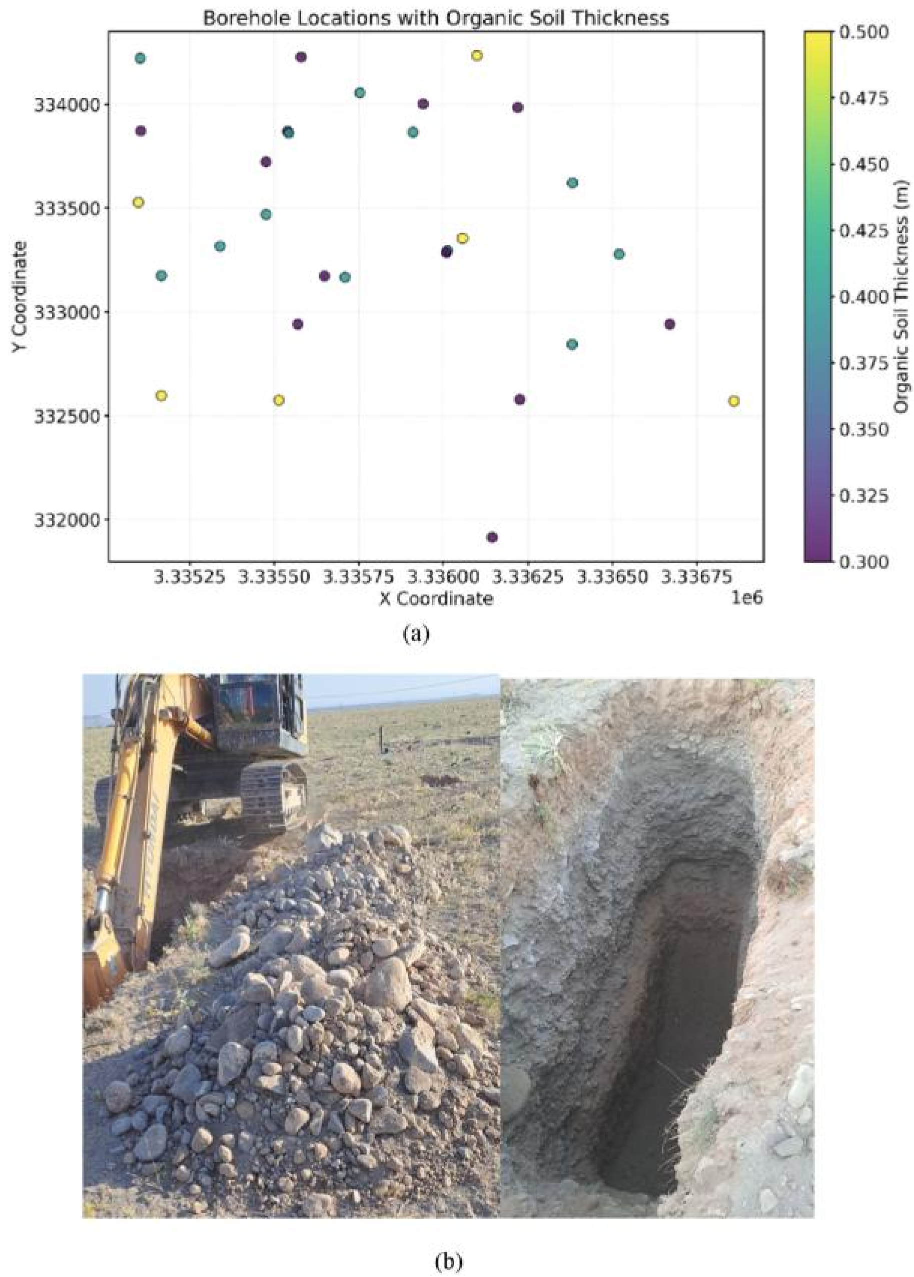

Fig. 4 (**a**) Borehole locations and organic soil thickness (m) (**b**) Granular soil at pile locations

differences in pile installation alignment, and possible micro-layer changes within the dense sand and gravel deposits. UNP 140 piles generally occupy the upper region of the scatter, reflecting the beneficial effect of increased section size on both L1 and L2 performance, whereas UNP 100 piles cluster in the lower capacity range. This analysis confirms that while L1 and L2 are related, the magnitude of strong-axis advantage is strongly dependent on section geometry and local geotechnical conditions.

3.4 Section and Depth Effects on L1 and L2 Capacities

3.4.1 Section Effect of Piles on L1 and L2

Figure 9 presents the influence of pile cross-section size (UNP 100 vs UNP 140) on final lateral load capacity for both L1 and L2 directions at two fixed embedment depths (120 cm and 170 cm). At both depths, L1 consistently exceeds L2 and UNP 140 piles generally outperform UNP 100 piles, reflecting the role of increased bending stiffness and cross-sectional area in mobilizing higher soil resistance. For most test pairs,

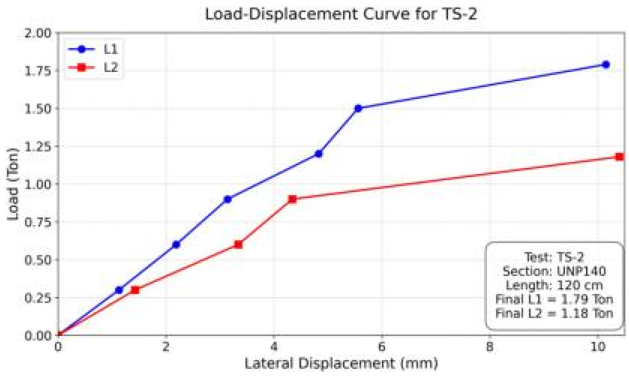

Fig. 5 Load displacement behavior of the piles (TS-2)

the improvement in L1 capacity with larger section size is more pronounced than in L2, highlighting the strong-axis advantage due to pile web orientation and reduced lateral flexibility. However, a few test pairs show relatively small gains—likely influenced by local variations in soil density, particle arrangement, and possible installation tolerances. This uniform trend across depths confirms that section geometry is a dominant contributor to lateral load capacity in dense granular soils.

3.4.2 Depth Effect of Piles on L1 and L2

Figure 10 illustrates the influence of embedment depth (120 cm vs. 170 cm) for each pile section size across L1 and L2 responses. Longer piles generally achieve higher final loads, particularly in L1, due to greater soil–pile contact length and increased mobilization of passive resistance at depth. For UNP 140 piles, depth enhancement in L1 is often larger than for UNP 100 piles, suggesting that deeper embedment more effectively exploits the stiffer section's capacity. Nevertheless, depth effect magnitude varies, with some test pairs showing modest or even negative differences in L2; such anomalies may be due to interlayer variability (e.g., loose sand pockets within the embedment range), differences in pile alignment, or localized changes in the p–y response. Overall, embedment depth is confirmed as a significant factor, but its benefit can be moderated by site-specific subsurface heterogeneity.

3.5 Comparison Between Section and Depth Effects on Pair Piles

Figure 11 directly compares the magnitude of capacity gain from section increase (UNP 140 – UNP 100) against that from depth increase (170–120 cm) for each test pair in L1 and L2 directions. This comparative trend analysis shows that section effect (red curves) is generally more dominant than depth effect (black curves) across most pairs, especially for L1, where section improvement frequently exceeds 0.8 T while depth effect often remains below 0.4 T. For L2, section effect still leads but with reduced margins, while depth effect occasionally matches or surpasses section improvement in isolated pairs. The variation in relative influence can be attributed to combined factors: the mechanical advantage of

Fig. 6 Final lateral load of the piles (UNP 100—L1)

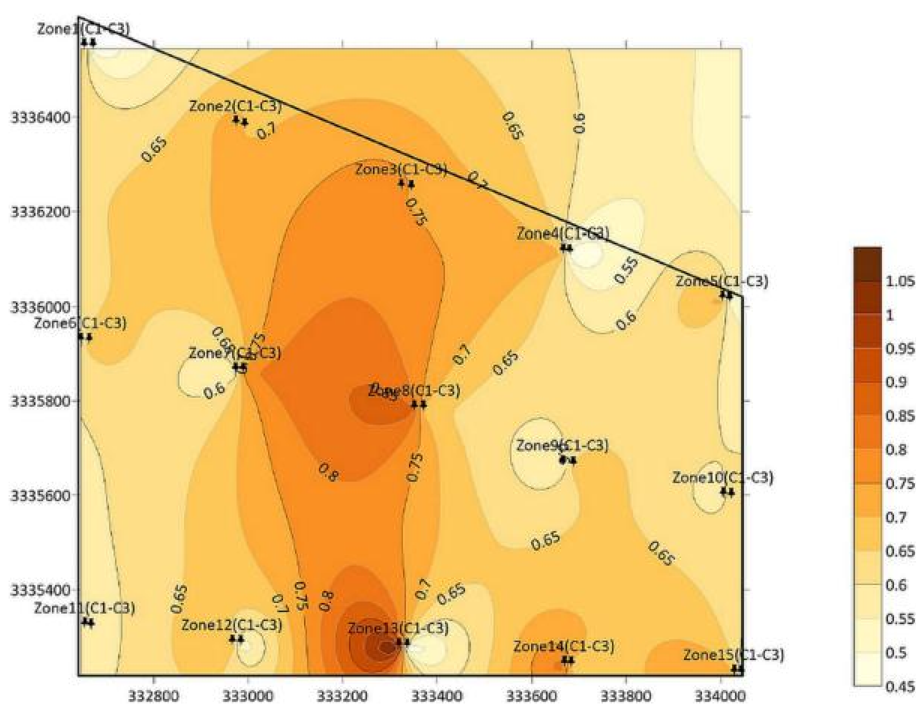

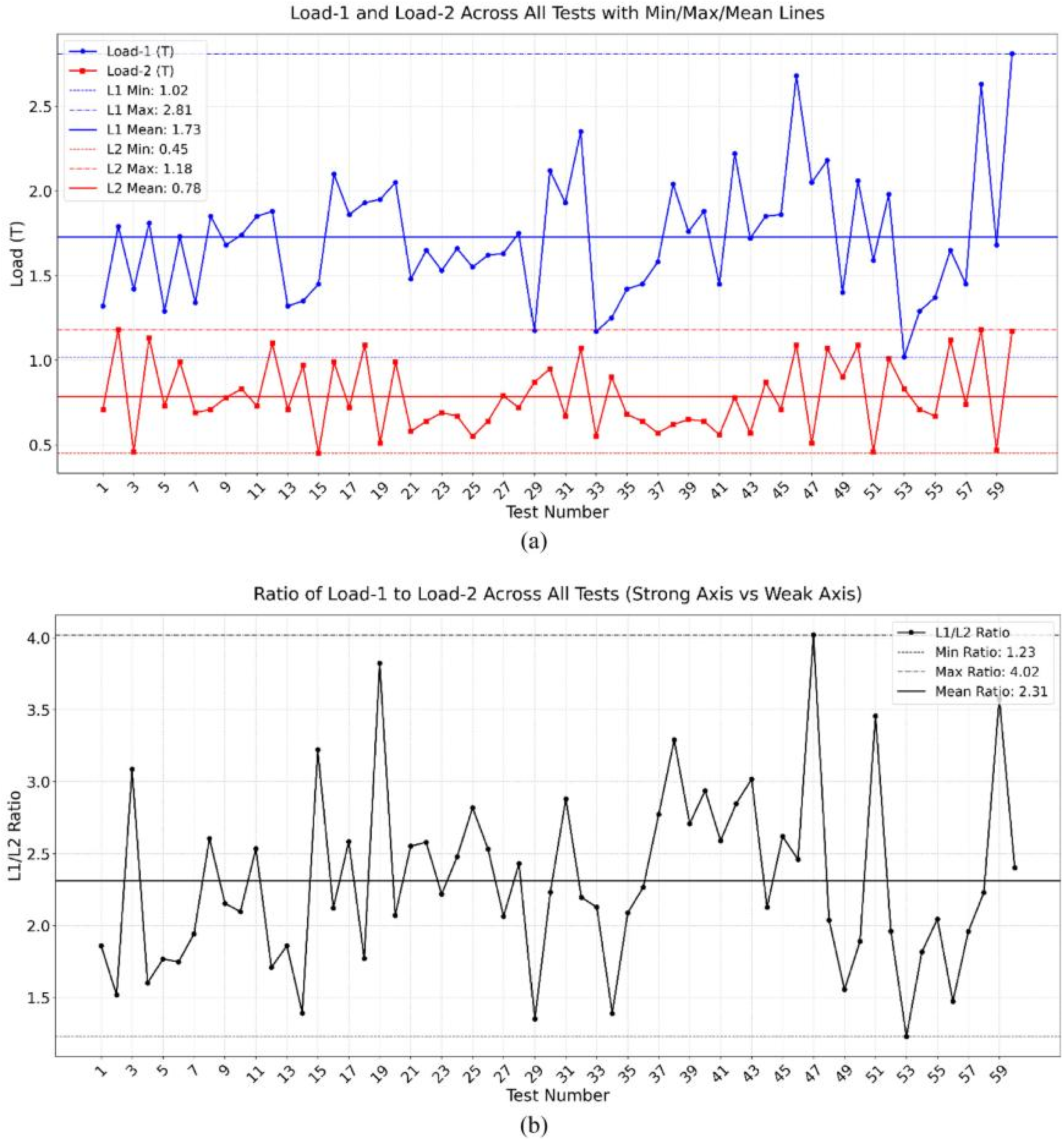

Fig. 7 (**a**) Final loads of the piles (L1 and L2) (**b**) L1/L2 ratio

larger cross-sections under bending, variability in soil stiffness with depth, and differences in mobilized side resistance. Notably, in a few cases depth effect is negative, meaning the longer pile carried less load—suggesting possible structural settlement effects, soil layering with weaker zones at greater depth, or testing-related variability. This side-by-side comparison helps identify which parameter is more efficient for increasing capacity under site conditions and provides guidance for foundation optimization in similar dense sand profiles.

The observed lateral load–displacement responses reflect the combined effects of soil stress transfer mechanisms and anisotropic pile stiffness rather than geotechnical failure.

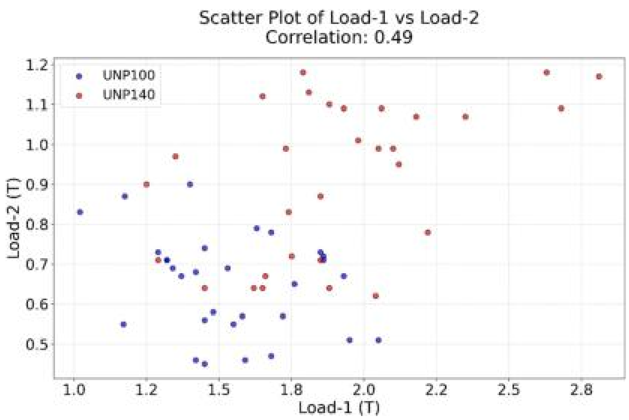

Fig. 8 Correlation between L1 and L2 of the piles

Across all tests, the absence of abrupt load drops or excessive rotations confirms that none of the piles reached ultimate soil failure, and that the reported capacities correspond to a serviceability-controlled response regime. In dense granular soils, lateral loading initially mobilizes passive earth pressures near the ground surface, resulting in high initial stiffness, followed by progressive stress redistribution along the embedded length as displacement increases. This behavior is consistent with classical soil–pile interaction principles underlying Broms' method for short rigid piles in cohesionless soils. The pronounced difference between strong and weak-axis responses reflects directional variation in bending stiffness, which governs how lateral stresses are transferred from the pile to the surrounding soil mass. Sensitivity to key parameters was implicitly captured through systematic variation of pile section size, embedment depth, and site-specific friction angle across 60 independent tests, revealing that L1 behavior is predominantly soil-controlled through mobilized shear strength, while L2 behavior is structurally controlled by section stiffness.

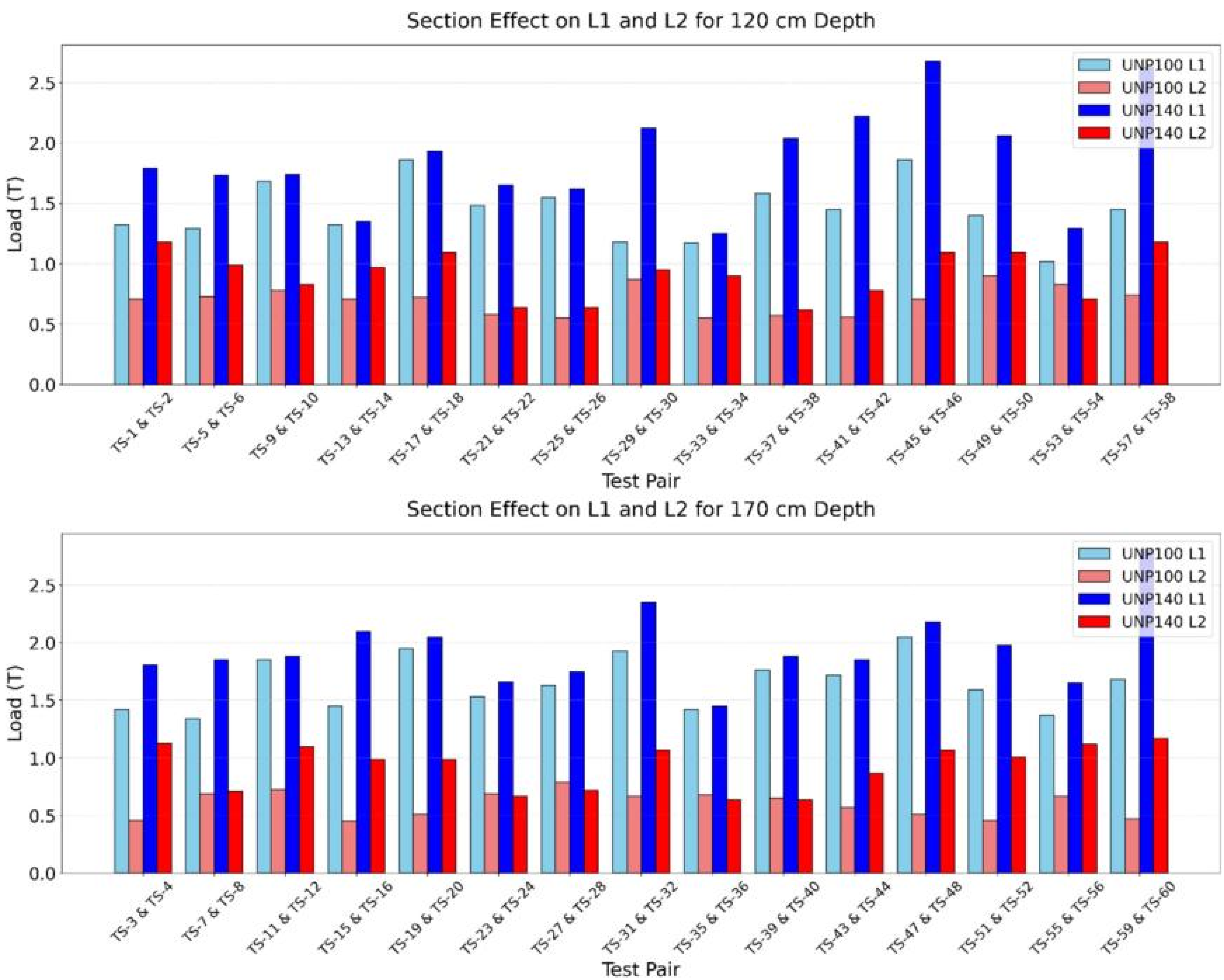

Fig. 9 Section effect of piles on L1 and L2

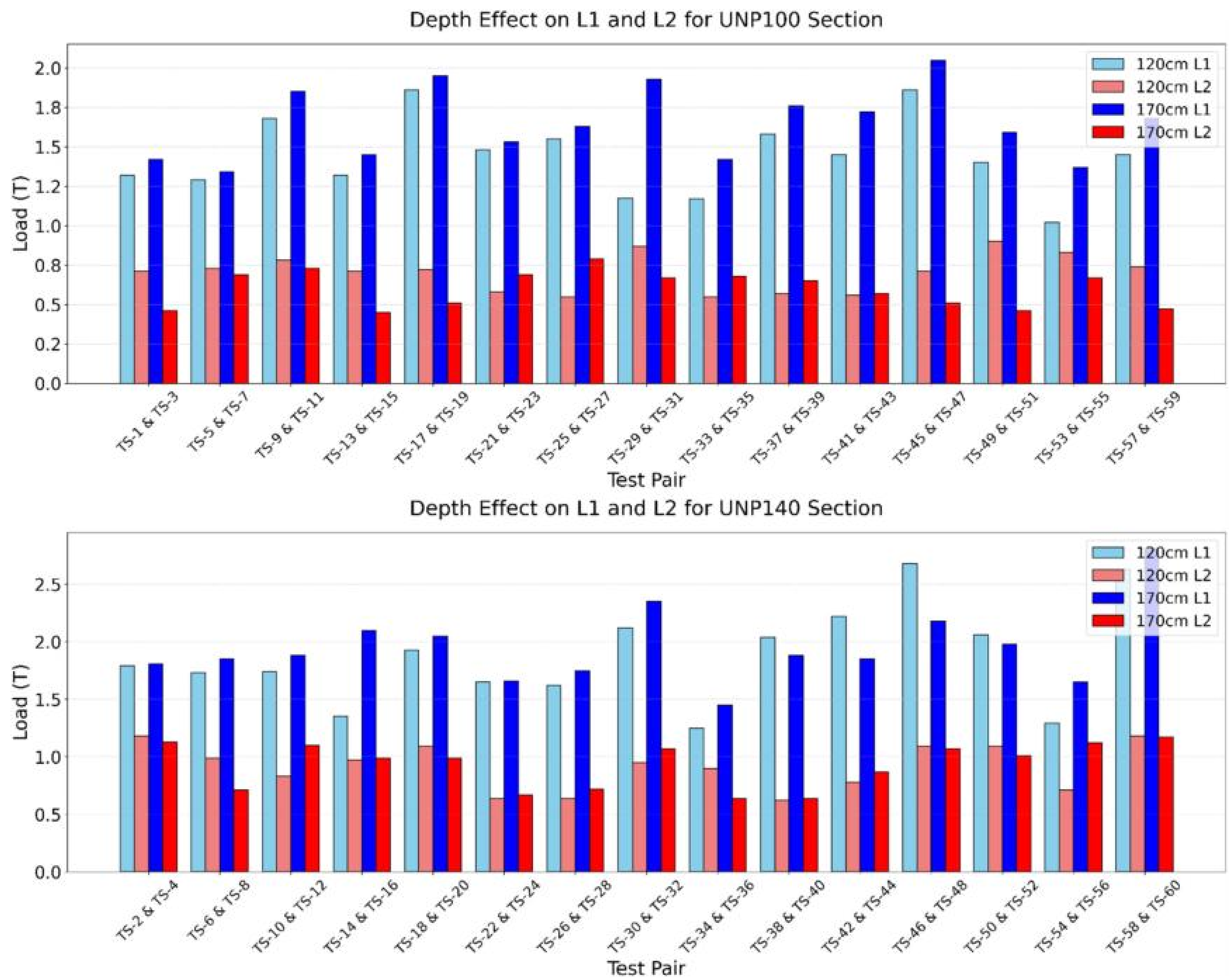

Fig. 10 Depth effect of piles on L1 and L2

3.6 Correlation of L1 and L2 with Friction Angle

The application of machine learning and data-driven approaches for correlating geotechnical properties and foundation performance has been widely reported in literature [39–43], demonstrating strong potential for capturing complex, nonlinear soil–structure interactions. However, the reliability of such models fundamentally depends on the availability of high-quality field data and physically meaningful input parameters, such as friction angle and measured lateral capacity.

In this section, the relationships between the strong-axis (L1) and weak-axis (L2) lateral capacities and the average soil friction angle are examined using quadratic regression analysis. The friction angle adopted for each test corresponds to the average value over the pile embedment depth, ensuring that the regression captures the overall shear strength mobilized by the pile–soil system under lateral loading, rather than being unduly influenced by localized variations within individual soil layers.

Figure 12 (a) and (b) presents the fitted correlations of L1–φ and L2–φ, respectively, for the full set of 60 pile tests. Figure 12 (a) shows the variation of L1 with friction angle, together with the best-fit second-degree polynomial and its associated statistical indicators (MSE and R2). The results indicate that L1 exhibits a clear and consistent increasing trend with friction angle, and the relatively high R2 value (0.9326) confirms a strong correlation between L1 and φ. This suggests that, under strong-axis loading, the lateral resistance of the piles is strongly governed by the mobilized shear strength of the surrounding dense granular soil, and that the adopted friction angle is an effective descriptor for capturing site-specific lateral capacity in the L1 direction.

By contrast, Fig. 12 (b) presents the corresponding correlation for the weak-axis direction (L2). Although a quadratic trend is discernible, the data scatter is noticeably larger,

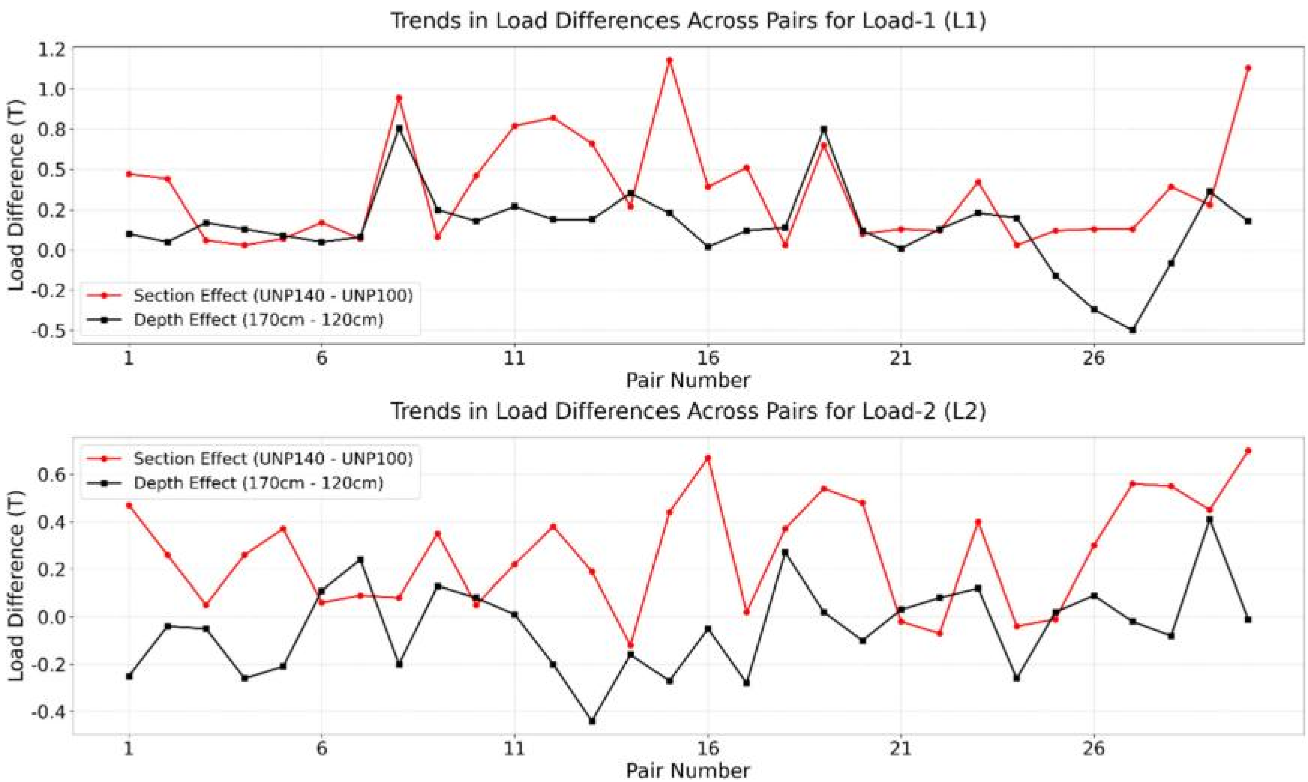

Fig. 11 Comparison between section and depth effect on pair piles

resulting in a significantly lower R^2 value compared to the strong-axis results. This weaker correlation implies that weak-axis capacity is less sensitive to variations in soil friction angle and is instead dominated by structural characteristics, specifically the lower bending stiffness about the minor axis. Collectively, these results highlight a critical distinction in design: while the soil friction angle is a reliable parameter for predicting L1, it is insufficient on its own to characterize L2 behavior, where section geometry and loading direction play the primary roles.

3.7 Comparison of Experimental Results with Theoretical Ultimate Capacity

In the design of solar panel foundations, verifying that the service loads remain well within the ultimate geotechnical capacity is essential for ensuring long-term alignment and stability. It is important to note that throughout the experimental program, none of the tested piles experienced complete geotechnical failure (plunging or excessive rotation). The lateral capacities reported in previous sections (L1 and L2) were defined at a specific serviceability limit state of 10 mm displacement, rather than at the ultimate soil failure point.

To contextualize these service-level capacities against the theoretical ultimate resistance of the soil, a comparative analysis was performed using Broms' method (1964) [43] for short rigid piles in cohesionless soil (Eq. 1). The theoretical ultimate lateral capacity (H_u) was calculated for each pile location using the specific friction angle (ϕ) and the corresponding Rankine passive earth pressure coefficient (K_p) derived from the geotechnical investigation.

$$H_u = \frac{0.5.\gamma.D.L^3.K_p}{e + L} \tag{1}$$

where:γ = Unit weight of soilD = Pile diameter (0.30 m).L = Embedment depth (1.2 m or 1.7 m).Kp = Rankine Passive Earth Pressure Coefficiente = Load eccentricity (height of the load application point above ground level)

For this comparison, the analysis focuses specifically on the relationship between the weak-axis capacity (L2) and the theoretical ultimate capacity (H_u). The strong-axis capacity (L1) was excluded from this specific comparison because, as demonstrated in Sect. 3.4.1, L1 behavior is heavily dominated by the "section effect" (the high bending stiffness of the steel core) rather than being purely governed by soil failure mechanisms. Conversely, L2 represents the critical design scenario where the structural stiffness is lower, making the comparison with soil ultimate capacity more relevant for safety assessments.

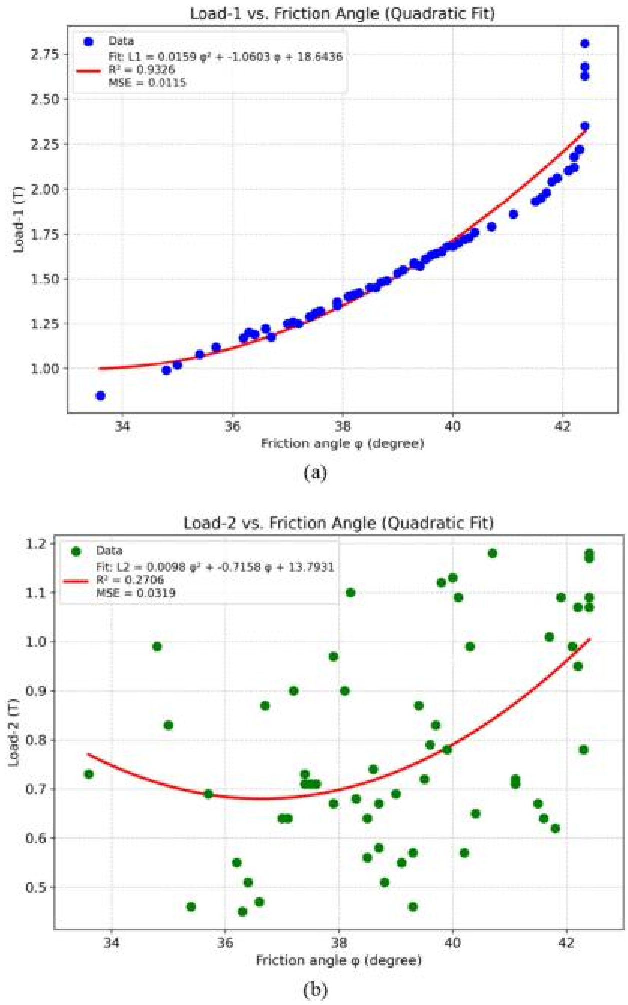

Fig. 12 Correlation of L1 and L2 with Friction Angle (**a**) L1 (**b**) L2

Figure 13 presents the ratio $\left(L2/H_{U(\text{Broms})}\right)$ for all 60 tests. The horizontal line at Ratio = 1.0 represents the theoretical failure point where the applied load equals the ultimate soil resistance. As illustrated, all calculated ratios fall below 1.0, ranging from approximately 0.16–0.87. This confirms that at the restrictive displacement limit of 10 mm, the piles mobilize only a fraction of the soil's ultimate theoretical resistance. Consequently, designing based on a 10 mm deflection limit inherently provides a significant factor of safety against geotechnical failure, particularly for composite piles where the internal steel core provides additional reserve capacity.

4 Practical Implications

The findings of this study have direct implications for the design of solar photovoltaic pile foundations in dense granular soils. The pronounced anisotropy observed between strong-axis (L1) and weak-axis (L2) lateral resistance highlights the importance of pile orientation relative to dominant wind loading directions. From a practical standpoint, the strong correlation between L1 capacity and soil friction angle indicates that site-specific geotechnical investigations can reliably inform strong-axis design using measured shear strength parameters. Conversely, the weak correlation between L2 capacity and friction angle demonstrates that increasing embedment depth alone is not an efficient strategy for improving weak-axis performance; instead, selecting an appropriate steel core section with sufficient bending stiffness is more effective. The comparison with Broms' theoretical ultimate capacity further confirms that adopting a serviceability displacement limit of 10 mm provides a substantial safety margin against geotechnical failure, supporting conservative yet economical foundation design for large-scale solar farms.

5 Limitations of the Study

The results presented in this study are derived from full-scale lateral load tests conducted at a single solar farm site characterized by dense granular soils with friction angles ranging from 32° to 43°. As such, the empirical correlations and behavioral trends identified herein are specific to dense sands and gravels and should not be directly extrapolated to cohesive soils, loose sands, or highly stratified deposits without additional verification. The experimental program was limited to static monotonic lateral loading applied under free-head conditions, typical of serviceability-controlled solar foundation behavior. Cyclic loading, long-term degradation, combined vertical–lateral loading, and environmental effects such as moisture variation were beyond the scope of the study. Furthermore, only two steel core section sizes (UNP 100 and UNP 140) and two embedment depths (1.2 m and 1.7 m) were investigated. While these configurations are representative of common solar foundation practice, broader parametric ranges would be required to generalize the findings to other foundation systems or loading regimes.

6 Future Recommendations

Future investigations should extend the experimental framework to other ground conditions, including loose sands, silty sands, and cohesive soils, where pile–soil interaction mechanisms and mobilization of lateral resistance may differ substantially. Additional full-scale tests incorporating deeper embedment depths, alternative steel core geometries, and varying pile diameters would help refine the proposed design trends and assess scalability. Moreover, cyclic and combined vertical–lateral loading conditions representative

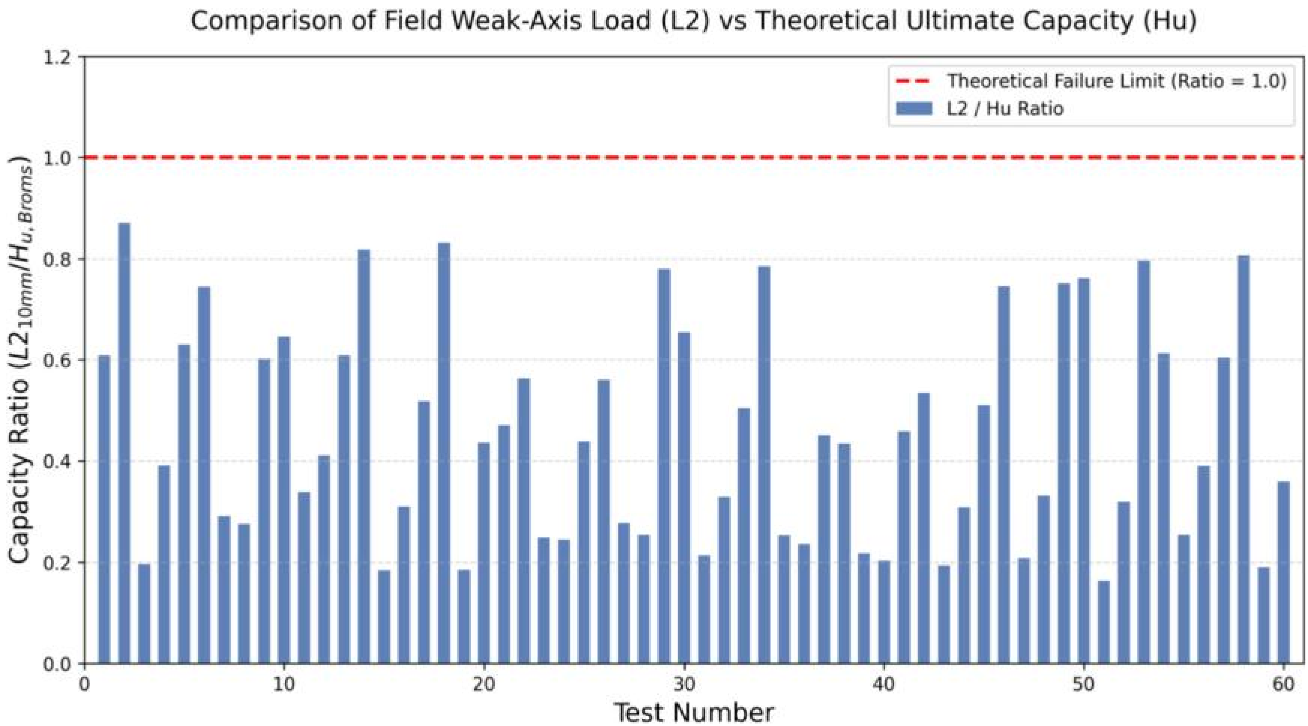

Fig. 13 Comparison of measured weak-axis service loads with theoretical ultimate capacities

of long-term wind action, temperature effects, and operational fatigue should be evaluated to better capture in-service performance. Integration of advanced numerical modeling calibrated against expanded field datasets is also recommended to support parametric studies and facilitate broader application of the proposed design framework for solar photovoltaic foundation systems.

7 Conclusions

This study presented a comprehensive full-scale field investigation into the lateral load–deformation behavior of composite concrete-encased steel piles used for solar photovoltaic foundations in dense granular soils at the Meymand Solar Farm, Iran. Based on the analysis of 60 full-scale tests on piles with varying core section sizes (UNP 100 and UNP 140), embedment depths (1.2 m and 1.7 m), and site-specific friction angles, the following conclusions are drawn:

• Lateral resistance exhibited pronounced anisotropy, with strong-axis (L1) capacities consistently exceeding weak-axis (L2) capacities for all configurations. The average L1/L2 ratio of 2.31 confirms that pile orientation relative to the dominant wind load direction is a governing factor in solar foundation design.

• Increasing the steel core section size from UNP 100 to UNP 140 produced larger and more consistent gains in lateral capacity than increasing embedment depth. This section effect was particularly dominant for L1 loading, yielding improvements of approximately 0.8 T at the serviceability limit, whereas the depth effect was more variable and, in some cases, negligible due to local soil heterogeneity.

• Quadratic regression analysis demonstrated a strong and statistically significant correlation ($R^2 = 0.9326$) between L1 capacity and soil friction angle (ϕ), indicating that strong-axis resistance is primarily governed by the mobilized shear strength of the surrounding dense granular soil. In contrast, L2 capacity showed a weak correlation with friction angle, confirming that weak-axis behavior is mainly controlled by the structural bending stiffness of the steel core section.

• Comparison of measured weak-axis service loads (L2 at 10 mm displacement) with theoretical ultimate capacities derived from Broms' method yielded utilization ratios ranging from 0.16 to 0.87. This confirms that the adopted serviceability displacement criterion effectively limits mobilized resistance to well below the ultimate geotechnical failure load, providing a substantial safety margin.

• Overall, the results support a decoupled design approach for composite solar piles in dense granular soils: strong-axis capacity can be reliably predicted using site-specific friction angle measurements, while weak-axis capacity should be controlled primarily through appropriate selection of steel core section size rather than increased embedment depth.

Author's Contributions Conceptualization: Iman Golpazir, Methodology: Reza Akherati and Anahita Akherati, Formal analysis: Ali Dehghanbanadaki, Writing: Alireza Rezaee.

Funding This research did not receive any funding.

Data Availability Data will be made available upon reasonable request.

Declarations:

Conflict of interest The authors declare that there is no conflict of interest in presenting this manuscript.

Consent for Publication This study does not include identifiable information about individuals or entities.

Ethics Approval and Consent to Participate This research did not involve the participation of human subjects.

References

1. Omar, S.M.; Khalifa, W.M.; Oz, T.: From fossil dependence on sustainability: the effects of energy transition, green growth, and financial inclusion on environmental degradation in the MENA region. Energies **18**(14), 3668 (2025). https://doi.org/10.3390/en18143668
2. Eyuboglu, K.; Uzar, U.: The social, economic, and environmental drivers of renewable energy: is income inequality a threat to renewable energy transition? J. Clean. Prod. **490**, 144780 (2025). https://doi.org/10.1016/j.jclepro.2025.144780
3. Mahadevan, V.; Rusho, M.A.; Yishak, S.: Critical review of energy storage systems: a comparative assessment of mechanisms, advantages, challenges, and integration with renewable energy. Results. Eng. (2025). https://doi.org/10.1016/j.rineng.2025.105589
4. Karipoğlu, F.; Denizli, O.: Towards renewable energy islands in Türkiye: potential and challenges. Renew. Sustain. Energy Rev. **211**, 115324 (2025). https://doi.org/10.1016/j.rser.2024.115324
5. Basem, A.; Opakhai, S.; Elbarbary, Z.M.S.; Atamurotov, F.; Benti, N.E.: A comprehensive analysis of advanced solar panel productivity and efficiency through numerical models and emotional neural networks. Sci. Rep. **15**(1), 259 (2025). https://doi.org/10.1038/s41598-024-70682-2
6. Priya, P.; Stonier, A.A.: Emerging innovations in solar photovoltaic (PV) technologies: the perovskite solar cells and more. Energy Rep. **14**, 216–242 (2025). https://doi.org/10.1016/j.egyr.2025.06.003
7. Sadat, S.A.; Pearce, J.M.: Techno-economic evaluation of electricity pricing structures on photovoltaic and photovoltaic-battery hybrid systems in Canada. Renew. Energy **242**, 122456 (2025). https://doi.org/10.1016/j.renene.2025.122456
8. Soltani, A.; Imani, M.A.; Imani, M.S.: Comprehensive strategic assessment of Iran's renewable energy potentials through a hybrid multi-criteria decision-making approach. Renew. Energy **1**(256), 123896 (2026). https://doi.org/10.1016/j.renene.2025.123896
9. Fathi, A.; Zaker, S.E.; Razeghi, M.; Yousefi, H.; Abdoos, M.; Amirizanjiran, M.: Optimization of solar panel installation structure to increase received radiation in Iran: an approach based on reducing structural diversity. Energy Convers. Manag. X. (2025). https://doi.org/10.1016/j.ecmx.2025.101282
10. Zahedi, R.; Sadeghitabar, E.; Khazaee, M.; Faryadras, R.; Ahmadi, A.: Potentiometry of wind, solar and geothermal energy resources and their future perspectives in Iran. Environ. Dev. Sustain. **27**(7), 15311–15337 (2025). https://doi.org/10.1007/s10668-024-04633-2
11. Panbechi, B.; Hajinezhad, A.; Moosavian, S.F.; Fattahi, R.: Enhancing the enviro-economic viability of biogas-solar hybrid systems: strategies for sustainable energy development in Iran. Energy Strategy Rev. **58**, 101671 (2025). https://doi.org/10.1016/j.esr.2025.101671
12. Opie, B.; Avci, O.; Gutta, J.B.; Quaranta, J.D.; Taylor, S.: A brief review of solar panel installations on former mine lands: technical challenges and uncertainties for tracking and foundation systems. Sol. Energy **300**, 113858 (2025). https://doi.org/10.1016/j.solener.2025.113858
13. Yang, H.; Yin, Y.; AbuSiada, A.: A comprehensive review of solar panel performance degradation and adaptive mitigation strategies. IET Control Theory Appl. **19**(1), e70040 (2025). https://doi.org/10.1049/cth2.70040
14. Zhang, J.; Li, R.; Yang, S.; Liu, J.; Guo, Z.; Feng, L.; Shang, W.; Zhu, L.; Du, B.: Field load testing and numerical analysis of offshore photovoltaic steel pipe piles. Soil Dyn. Earthq. Eng. **188**, 109034 (2025). https://doi.org/10.1016/j.soildyn.2024.109034
15. Fu, S.; Chen, H.; Lv, G.E.; Jia, X.; Li, X.: Experimental and numerical research on p–y curve of offshore photovoltaic pile foundations on sandy soil foundation. J. Mar. Sci. Eng. **13**(10), 1959 (2025). https://doi.org/10.3390/jmse13101959
16. Thangavel, J.K.; Rathod, D.: Behaviour of a laterally loaded rigid pile subjected to one-way cyclic loading. Geotech. Geol. Eng. **42**(6), 4931–4951 (2024). https://doi.org/10.1007/s10706-024-02822-4
17. Chandaluri, V.K.; Sawant, V.A.: Response of laterally loaded single pile in clayey slope for large displacements. Geotech. Geol. Eng. **42**(1), 153–164 (2024). https://doi.org/10.1007/s10706-023-02562-x
18. Reese, L.C.; Van Impe, W.; Wang, S.T.: Single piles and pile groups under lateral loading. CRC Press (2025)
19. Cheng, X.; Li, M.; Li, Q.; Lu, D.; Du, X.: Dynamic response and fatigue damage analysis of offshore wind turbines supported by four-pile jacket in clays under typhoons. Acta Geotech. **20**(5), 2461–2481 (2025). https://doi.org/10.1007/s11440-024-02526-2
20. Shao, L.; Qia, H.; Zhu, Z.; Guo, Y.: Numerical simulation study of fatigue damage in high pile cap foundation for offshore wind power. Structures **74**, 108627 (2025). https://doi.org/10.1016/j.istruc.2025.108627
21. Tarenia, K.; Patra, N.R.: Long-term effect of vertical and lateral loads on piled raft foundations: a case study. Proc. Inst. Civ. Eng. Geotech. Eng. **177**(4), 337–349 (2024). https://doi.org/10.1680/jgeen.22.00030
22. Wang, C.; Ding, X.; Liu, H.; Zhang, Y.; Cao, G.; Wang, Z.: Centrifuge model tests on bearing behavior of lateral-loaded single pile in coral sand. Acta Geotech. **19**(7), 4581–4603 (2024). https://doi.org/10.1007/s11440-023-02096-9
23. Guo, J.; Jia, X.; Fu, Y.; Wang, Z.: Lateral deformation calculation of bridge pile foundation subjected to horizontal dynamic load. Int. J. Struct. Stab. Dyn. **3**, 2650158 (2025). https://doi.org/10.1142/S0219455426501580
24. Ren, S.; Kong, D.; Du, Y.; Chen, Y.; Zhu, B.: Numerical modeling of multi-directional lateral behaviour of pile foundations for offshore wind turbines in clay. Ocean Eng. **338**, 121817 (2025). https://doi.org/10.1016/j.oceaneng.2025.121817
25. Phatsak, T.; Kongkitkul, W.; Krajangphon, P.: Influence of orientation angle on the lateral behavior and efficiency of 2 × 2 and 3 × 3 pile groups based on 1-g physical model tests. Arab. J. Sci. Eng. (2025). https://doi.org/10.1007/s13369-025-10067-3
26. Chen, H.; Wang, Y.; Zhang, C.; Yi, L.; Ma, Z.; Ye, T.: Model testing of pile-anchor combined foundation under tensile-bending and compressive-bending loading. Arab. J. Sci. Eng. (2025). https://doi.org/10.1007/s13369-025-10126-9

27. Xu, D.S.; Xu, X.Y.; Li, W.; Fatahi, B.: Field experiments on laterally loaded piles for an offshore wind farm. Mar. Struct. **69**, 102684 (2020). https://doi.org/10.1016/j.marstruc.2019.102684
28. Li, W.; Yuan, W.; Tao, Q.; Gong, W.; Dai, G.: The influence of pile shaft distributed grouting on the horizontal load response of rectangular piles. KSCE J. Civ. Eng. **28**(12), 5516–5523 (2024). https://doi.org/10.1007/s12205-024-2727-3
29. Krishnanunni, K.T.; Rathod, D.: The numerical investigation on the efficacy of a laterally loaded finned pile installed in a two-layered sandy slope. Int. J. Geotech. Eng. **19**(4), 213–228 (2025). https://doi.org/10.1080/19386362.2025.2469964
30. Liu, W.; Li, H.; Weng, X.; Wang, Z.; Chen, Q.; Lei, Y.; Li, X.; Xiang, H.; Yuan, B.; Hu, W.; Xu, X.; Feng, Y.: Numerical study on the effect of pile shape and loading direction on the lateral response of displacement pile in sand. Sci. Rep. **15**(1), 26653 (2025). https://doi.org/10.1038/s41598-025-11902-1
31. Golpazir, I.; Dehghanbanadaki, A.; Akherati, R.; Akherati, A.: Effect of installation method on the uplift capacity of single driven steel piles: full-scale field study. Indian Geotech. J. **55**(3), 1981–1993 (2025). https://doi.org/10.1007/s40098-024-01083-5
32. Su, D.; Yan, W.M.: A multidirectional p–y model for lateral sand–pile interactions. Soils Found. **53**(2), 199–214 (2013). https://doi.org/10.1016/j.sandf.2013.02.002
33. Truong, P.; Lehane, B.M.: Effects of pile shape and pile end condition on the lateral response of displacement piles in soft clay. Géotechnique **68**(9), 794–804 (2018). https://doi.org/10.1680/jgeot.16.P.291
34. Elkasabgy, M.; El Naggar, M.H.: Lateral performance and p–y curves for large-capacity helical piles installed in clayey glacial deposit. J. Geotech. Geoenviron. Eng. **145**(10), 04019078 (2019). https://doi.org/10.1061/(ASCE)GT.1943-5606.0002063
35. Hamderi, M.: Finite element-based p–y curves in sand. Arab. J. Sci. Eng. **48**(10), 14183–14194 (2023). https://doi.org/10.1007/s13369-023-08121-z
36. Ge, C.; Shen, J.; Zhan, Y.; Chen, D.: A modified p–y model considering local scour effects for monopile foundations in soft clays. Bull. Eng. Geol. Environ. **83**(9), 351 (2024). https://doi.org/10.1007/s10064-024-03852-1
37. Ding, X.; Liu, J.; Li, X.; Wang, C.; Liu, H.; Ou, Q.: Lateral bearing characteristics and p–y model of single pile in coral sand considering effect of vertical load. Ocean Eng. **342**, 122886 (2025). https://doi.org/10.1016/j.oceaneng.2025.122886
38. Xue, X.; Liu, L.; Li, M.; Han, J.; Deng, F.; Long, B.: Mechanical properties and p–y curve of rock slope–pile system under horizontal load. J. Build. Eng. (2025). https://doi.org/10.1016/j.jobe.2025.114071
39. Zhou, J.; Koopialipoor, M.; Li, E.; Armaghani, D.J.: Prediction of rockburst risk in underground projects developing a neuro-bee intelligent system. Bull. Eng. Geol. Environ. **79**(8), 4265–4279 (2020). https://doi.org/10.1007/s10064-020-01788-w
40. Barkhordari, M.; Armaghani, D.J.; Asteris, P.G.: Structural damage identification using ensemble deep convolutional neural network models. Comput. Model. Eng. Sci. **134**(2), 835–852 (2023). https://doi.org/10.32604/cmes.2022.020840
41. Barkhordari, M.S.; Armaghani, D.J.; Mohammed, A.S.; Ulrikh, D.V.: Data-driven compressive strength prediction of fly ash concrete using ensemble learner algorithms. Buildings **12**(2), 132 (2022). https://doi.org/10.3390/buildings12020132
42. Zhou, J.; Guo, H.; Koopialipoor, M.; Jahed Armaghani, D.; Tahir, M.M.: Investigating the effective parameters on the risk levels of rockburst phenomena by developing a hybrid heuristic algorithm. Eng. Comput. **37**(3), 1679–1694 (2021). https://doi.org/10.1007/s00366-019-00908-9
43. Broms, B.B.: Lateral resistance of piles in cohesionless soils. J. Soil Mech. Found. Div. **90**(3), 123–156 (1964). https://doi.org/10.1061/JSFEAQ.0000614